Electronic Supplementary Material (ESI) for Physical Chemistry Chemical Physics.


# Supplementary Information

## Adiabatic Quantum Computing with Spin Qubits Hosted by Molecules

Satoru Yamamoto, Shigeaki Nakazawa, Kenji Sugisaki, Kazunobu Sato,*
Kazuo Toyota, Daisuke Shiomi, and Takeji Takui,*

**Table of Contents**

## 1. The spin Hamiltonian in ESR-QC systems

In this section, we introduce quantum mechanical treatments for a three electron (3e) system and one electron and two nuclear (1e+2n) system in ESR-QC experiments.

**1.1.** The spin Hamiltonian of the three electron (3e) molecular spin quantum computer**.**

The spin Hamiltonian of the 3e system in oriented media can be written by Eq. (S.1-1) in Schrödinger picture.

$$\hat{H}_{3e} = \sum_{i=1}^{3} \hat{\boldsymbol{S}}^i g^i \beta \boldsymbol{B} + \sum_{i<j}^{3,3} \hat{\boldsymbol{S}}^i (J+D)^{ij} \hat{\boldsymbol{S}}^j \qquad \text{Eq. (S.1-1)}$$

Here, $\hat{\boldsymbol{s}}^i$ is a spin operator and $g^i$ is a *g*-tensor of the *i*th electron and $\beta_e$ is Bohr magneton. The interaction tensors between spins are assumed to be exchange interaction ( $J^{ij}$ ) and spin-dipole interaction ( $D^{ij}$ ). Applying the static magnetic field $\boldsymbol{B} = (0,0,B_z)$ , the spin Hamiltonian is described by Eq. (S.1-2).

$$\hat{H}_{3e} = \sum_{i=1}^{3} \left( \sum_{k=x,y,z} \hat{S}_k^i g_{kz}^i \beta_e B_z \right) + \sum_{i<j}^{3,3} \hat{\boldsymbol{S}}^i (J+D)^{ij} \hat{\boldsymbol{S}}^j \qquad \text{Eq. (S.1-2)}$$

In order to transform the individual rotational frame (=interaction picture), the Larmor frequency ( $\omega_0$ ) of *i*th spin is selected under the condition of $\omega_0^i = g_{zz}^i \beta_e B_z / \mathsf{h}$ , then the interaction Hamiltonian is described by Eqs. (S.1-3, S.1-4, S.1-5).

$$\hat{H}_{3e}^0 = \sum_{i=1}^{3} \mathsf{h}\omega_0 \hat{S}_z^i \qquad \text{Eq. (S.1-3)}$$

$$\hat{H}_{3e}^{int} = \sum_{i=1}^{3} \left( \sum_{k=x,y} \hat{S}_k^i(t) g_{kz}^i \beta_e B_z \right) + \sum_{i<j}^{3,3} \left( \sum_{k,l=x,y,z} \hat{S}_k^i(t) (J+D)_{kl}^{ij} \hat{S}_l^j(t) \right) \qquad \text{Eq. (S.1-4)}$$

$$\hat{S}_x^i(t) = \cos(\omega_0^i t)\hat{S}_x^i - \sin(\omega_0^i t)\hat{S}_y^i \qquad \text{Eq. (S.1-5a)}$$

$$\hat{S}_y^i(t) = \sin(\omega_0^i t)\hat{S}_x^i + \cos(\omega_0^i t)\hat{S}_y^i \qquad \text{Eq. (S.1-5b)}$$

$$\hat{S}_z^i(t) = \hat{S}_z^i$$

Eq. (S.1-5c)

In the zeroth order secular approximation, the fast Larmor rotating terms in Eq. (S.1-4) are approximated as zero in the case of the small anisotropy of *g*-tensors and small interactions between spins (compared with the Larmor frequency). Therefore the spin Hamiltonian of the three electron system in the time evolution can be written by Eq. (S.1-6).

$$\hat{H}_{3e}^{int} = \sum_{i<j}^{3,3} \hat{S}_z^i (J+D)_{zz}^{ij} \hat{S}_z^j \qquad \text{Eq. (S.1-6)}$$

In the case of ESR experiments in solution, the same procedure can be executed by only changing the parameters of the tensor into the isotropic terms (Eq. (S.1-7)).

$$\hat{H}^{\text{int}}_{\text{3e, sol}} = \sum_{i<j}^{3,3} \hat{S}^i_z J^{ij}_{zz} \hat{S}^j_z \qquad \text{Eq. (S.1-7)}$$

**1.2.** The spin Hamiltonian of the one electron and two nuclear (1e+2n) molecular spin quantum computer**.**

The spin Hamiltonian of the 1e+2n system in single crystals can be written by Eq. (S.1-8) in Schrödinger picture.

$$\hat{H}_{\text{1e+2n}} = \hat{\boldsymbol{S}}^1 g^1 \beta_{\text{e}} \boldsymbol{B} - \sum_{i=2}^{3} \hat{\boldsymbol{I}}^i g^i \beta_{\text{n}} \boldsymbol{B} + \sum_{j=2}^{3} \hat{\boldsymbol{S}}^1 A^{1j} \hat{\boldsymbol{I}}^j + \hat{\boldsymbol{I}}^2 (J+D)^{23} \hat{\boldsymbol{I}}^3 \qquad \text{Eq. (S.1-8)}$$

Here, $\hat{S}^i$ and $\hat{\boldsymbol{I}}^i$ are spin operators and $g^i$ is a *g*-tensor of the *i*th spin and $\beta_{\text{e}}$ and $\beta_{\text{n}}$ is Bohr and nuclear magneton, respectively. The interaction tensors between spins are assumed to be hyperfine interaction ( $A^{1j}$ ), exchange interaction ( $J^{ij}$ ) and spin-dipole interaction ( $D^{ij}$ ). Applying the static magnetic field $\boldsymbol{B} = (0,0,B_z)$ , the spin Hamiltonian can be written by Eq. (S.1-9).

$$\hat{H}_{\text{1e+2n}} = \sum_{k=x,y,z} \hat{S}^1_k g^1_{kz} \beta_{\text{e}} B_z - \sum_{i=2}^{3} \left( \sum_{k=x,y,z} \hat{I}^i_k g^i_{kz} \beta_{\text{n}} B_z \right) + \sum_{j=2}^{3} \hat{\boldsymbol{S}}^1 A^{1j} \hat{\boldsymbol{I}}^j + \hat{\boldsymbol{I}}^2 (J+D)^{23} \hat{\boldsymbol{I}}^3 \qquad \text{Eq. (S.1-9)}$$

In order to transform the individual rotational frame (=interaction picture), the Larmor frequency ( $\omega_0$ ) of an *i*th spin is selected under the condition of $\omega^i_{0,\text{e}} = g^i_{zz} \beta_{\text{e}} B_z / \mathsf{h}$ and $\omega^i_{0,\text{n}} = -g^i_{zz} \beta_{\text{n}} B_z / \mathsf{h}$ , then the interaction Hamiltonian is represented by Eqs. (S.1-9, S.1-10, S.1-11, S.1-12).

$$\hat{H}^0_{\text{1e+2n}} = \mathsf{h}\omega^1_{0,\text{e}} \hat{S}^1_z + \sum_{i=2}^{3} \mathsf{h}\omega^i_{0,\text{n}} \hat{I}^i_z \qquad \text{Eq. (S.1-10)}$$

$$\hat{H}^{\text{int}}_{\text{1e+2n}} = \sum_{k=x,y} \hat{S}^1_k(t) g^1_{kz} \beta_{\text{e}} B_z - \sum_{i=2}^{3} \left( \sum_{k=x,y} \hat{I}^i_k(t) g^i_{kz} \beta_{\text{n}} B_z \right) + \sum_{j=2}^{3} \left( \sum_{k,l=x,y,z} \hat{S}^1_k(t) A^{1j}_{kl} \hat{I}^j_l(t) \right) + \sum_{k,l=x,y,z} \hat{I}^2_k(t) (J+D)^{23}_{kl} \hat{I}^3_l(t) \qquad \text{Eq. (S.1-11)}$$

$$\hat{S}^i_x(t) = \cos(\omega^i_{0,\text{e}} t) \hat{S}^i_x - \sin(\omega^i_{0,\text{e}} t) \hat{S}^i_y \qquad \text{Eq. (S.1-12a)}$$

$$\hat{S}^i_y(t) = \sin(\omega^i_{0,\text{e}} t) \hat{S}^i_x + \cos(\omega^i_{0,\text{e}} t) \hat{S}^i_y \qquad \text{Eq. (S.1-12b)}$$

$$\hat{S}^i_z(t) = \hat{S}^i_z \qquad \text{Eq. (S.1-12c)}$$

$$\hat{I}^i_x(t) = \cos(\omega^i_{0,\text{n}} t) \hat{I}^i_x - \sin(\omega^i_{0,\text{n}} t) \hat{I}^i_y \qquad \text{Eq. (S.1-13a)}$$

$$\hat{I}^i_y(t) = \sin(\omega^i_{0,\text{n}} t) \hat{I}^i_x + \cos(\omega^i_{0,\text{n}} t) \hat{I}^i_y \qquad \text{Eq. (S.1-13b)}$$

$$\hat{I}^i_z(t) = \hat{I}^i_z \qquad \text{Eq. (S.1-13c)}$$

In the zeroth order secular approximation, the fast Larmor rotating terms in Eq. (S.1-10) are approximated to be zero in the case of the small anisotropy of *g*-tensors and small interactions between spins (compared with the Larmor frequency). The difference from the 3e system occurs in the hyperfine tensor because these terms are not small enough compared with the Larmor frequency of nuclei. Then the spin Hamiltonian of the 1e+2n system in the time evolution can be written by Eq. (S.1-14).

$$\hat{H}^{\mathrm{int}}_{\mathrm{1e+2n}} = \sum_{j=2}^{3}\left( \sum_{l=x,y,z} \hat{S}^{1}_{z} A^{1j}_{zl} \hat{I}^{j}_{l}(t) \right) + \hat{I}^{2}_{z} (J+D)^{23}_{zz} \hat{I}^{3}_{z} \qquad \text{Eq. (S.1-14)}$$

Only when the static magnetic field is applied parallel to a principal axis of each hyperfine tensor, the Hamiltonian in time evolution operators can be written only by the scalar interactions by Eq. (S.1-15).

$$\hat{H}^{\mathrm{int}}_{\mathrm{1e+2n}} = \sum_{j=2}^{3} \hat{S}^{1}_{z} A^{1j}_{zz} \hat{I}^{j}_{z} + \hat{I}^{2}_{z} (J+D)^{23}_{zz} \hat{I}^{3}_{z} \qquad \text{Eq. (S.1-15)}$$

In the case of ESR experiments in solution, the same procedure can be executed by only changing the parameters of the tensor into the isotropic term. Therefore, there is no restriction on the relation between the static magnetic field and the hyperfine axis in a solution case (Eq. (S.1-16)).

$$\hat{H}^{\mathrm{int}}_{\mathrm{1e+2n,\,sol}} = \sum_{j=2}^{3} \hat{S}^{1}_{z} A^{1j}_{\mathrm{iso}} \hat{I}^{j}_{z} + \hat{I}^{2}_{z} J^{23} \hat{I}^{3}_{z} \qquad \text{Eq. (S.1-16)}$$

## 2. Generation of the AQC pulse sequence in single crystal systems.

The pulse sequence of AQC was calculated by an analytical method which allows to combine the single spin operations, two spin interactions and a three spin interaction. Here, we describe the calculation method of the pulse sequence. The assumed operation set is given in red and the other operations which are composed of the assumed operation set are denoted in black in the equations. In this calculation, arbitrary spin rotations (2α radian) around the x- and y-axes of each spin ( $\exp\left(-i\alpha\sigma_x^k\right)$,$\exp\left(-i\alpha\sigma_y^k\right)$) and time evolution of the Hamiltonian ( $H=\sum_{i<j}^{3}\alpha^{ij}\sigma_z^i\sigma_z^j$ ) was assumed. In the figure of the pulse sequence, the pulse operations are depicted in Figure S1. The time of the pulse interval is also shown between the pulses.

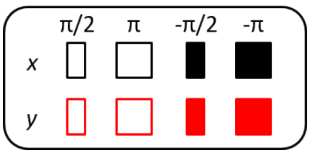


Figure S1. Notation of pulse operations. Black(red) blocks indicate the rotation around the *x*-(*y*-) axis. Square(oblong) blocks indicate the rotational angles of $\pi(\pi/2)$. The filled block means a minus angle operation. Other pulse operations around the *x*- and *y*- axes are written as blue blocks with a number/word.

**2.1**. Single spin operations.

The single spin operations of the z-direction can be replaced by Figure S2. This is because the arbitrary rotation around the z-axis can be written by Eqs. (S.2-1, S.2-2).

$$\exp\left(-i\alpha\sigma_z^k\right)=\exp\left(i\frac{\pi}{4}\sigma_y^k\right)\cdot\exp\left(-i\alpha\sigma_x^k\right)\exp\left(-i\frac{\pi}{4}\sigma_y^k\right) \qquad \text{Eq. (S.2-1)}$$

$$\exp\left(-i\alpha\sigma_z^k\right)=\exp\left(-i\frac{\pi}{4}\sigma_x^k\right)\cdot\exp\left(-i\alpha\sigma_y^k\right)\exp\left(i\frac{\pi}{4}\sigma_x^k\right) \qquad \text{Eq. (S.2-2)}$$


Figure S2. The pulse sequence of single spin operations. a) Corresponds to the Eq. (S.2-1). b) Corresponds to Eq. (S.2-2). Blue blocks of a and b are the 2α rotation around the *x*- and *y*- axes, respectively.

**2.2**. Two spin interactions.

The two spin interaction between $\sigma_z^i$ and $\sigma_z^j$ ($i \neq j$) is decomposed as given by Eqs. (S.2-3) and (S.2-4) or (S.2-5). The calculated pulse sequence corresponding to Eqs. (S.2-3a) with (S.2-4a) is shown in Figure S3.

In the three spin system, the operator $\exp(-i\alpha^{ij}\sigma_z^i\sigma_z^j t/\mathrm{h})$ can be written by Eqs. (S.2-3).

$$\exp(-i\alpha^{ij}\sigma_z^i\sigma_z^j t/\mathrm{h})|_{i\neq k\neq l} = \exp(-iHt/2\mathrm{h})\cdot\exp(-iH^{-k}t/2\mathrm{h}) \quad \text{Eq. (S.2-3a)}$$

$$= \exp(-iH^{-k}t/2\mathrm{h})\cdot\exp(-iHt/2\mathrm{h}) \quad \text{Eq. (S.2-3b)}$$

Here, $H = \sum_{i<j}^{3}\alpha^{ij}\sigma_z^i\sigma_z^j$ and $H^{-k} = \sum_{i<j}^{3}\alpha^{ij}\sigma_z^i\sigma_z^j|_{i\neq k\neq j} - \sum_{i\neq k}^{3}\alpha^{ik}\sigma_z^i\sigma_z^k$. The operator $\exp(-iH^{-k}t/\mathrm{h})$ can be achieved by Eqs. (S.2-4).

$$\exp(-iH^{-k}t/2\mathrm{h}) = \exp\left(-i\frac{\pi}{2}\sigma_x^k\right)\cdot\exp(-iHt/\mathrm{h})\cdot\exp\left(i\frac{\pi}{2}\sigma_x^k\right) \quad \text{Eq. (S.2-4a)}$$

$$= \exp\left(i\frac{\pi}{2}\sigma_x^k\right)\cdot\exp(-iHt/\mathrm{h})\cdot\exp\left(-i\frac{\pi}{2}\sigma_x^k\right) \quad \text{Eq. (S.2-4b)}$$

$$= \exp\left(-i\frac{\pi}{2}\sigma_y^k\right)\cdot\exp(-iHt/\mathrm{h})\cdot\exp\left(i\frac{\pi}{2}\sigma_y^k\right) \quad \text{Eq. (S.2-4c)}$$

$$= \exp\left(i\frac{\pi}{2}\sigma_y^k\right)\cdot\exp(-iHt/\mathrm{h})\cdot\exp\left(-i\frac{\pi}{2}\sigma_y^k\right) \quad \text{Eq. (S.2-4d)}$$

Any decomposed operation sets can be chosen for the pulse sequence in Eqs. (S.2-4). If you do not have to consider global phases, any pattern of $\pi$ pulses with the same direction is permitted as given by Eqs. (S.2-5).

$$-\exp(-iH^{-k}t/2\mathrm{h}) = \exp\left(-i\frac{\pi}{2}\sigma_x^k\right)\cdot\exp(-iHt/\mathrm{h})\cdot\exp\left(-i\frac{\pi}{2}\sigma_x^k\right) \quad \text{Eq. (S.2-5a)}$$

$$= \exp\left(i\frac{\pi}{2}\sigma_x^k\right)\cdot\exp(-iHt/\mathrm{h})\cdot\exp\left(i\frac{\pi}{2}\sigma_x^k\right) \quad \text{Eq. (S.2-5b)}$$

$$= \exp\left(-i\frac{\pi}{2}\sigma_y^k\right)\cdot\exp(-iHt/\mathrm{h})\cdot\exp\left(-i\frac{\pi}{2}\sigma_y^k\right) \quad \text{Eq. (S.2-5c)}$$

$$= \exp\left(i\frac{\pi}{2}\sigma_y^k\right)\cdot\exp(-iHt/\mathrm{h})\cdot\exp\left(i\frac{\pi}{2}\sigma_y^k\right) \quad \text{Eq. (S.2-5d)}$$

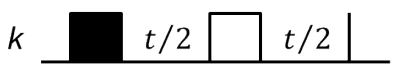


Figure S3. An example of the pulse sequence of a two spin interaction. The operation $\exp(-i\alpha^{ij}\sigma_z^i\sigma_z^j t/\mathrm{h})$ ($i \neq k, k \neq j, j \neq i$) is composed of Eqs. (S.2-3a) and (S.2-4a). The vertical line indicates the end of the pulse sequence.

In the case of the opposite sign operator ( $\exp(i\alpha^{ij}\sigma_z^i\sigma_z^j t/\mathrm{h})$ ), the operation can be written by Eqs. (S.2-6), utilizing an $\exp(-i\alpha^{ij}\sigma_z^i\sigma_z^j t/\mathrm{h})$ operation.

$$\exp(i\alpha^{ij}\sigma_z^i\sigma_z^j t/\mathrm{h}) = \exp\left(-i\frac{\pi}{2}\sigma_x^i\right)\cdot\exp(-i\alpha^{ij}\sigma_z^i\sigma_z^j t/\mathrm{h})\cdot\exp\left(i\frac{\pi}{2}\sigma_x^i\right) \quad \text{Eq. (S.2-6a)}$$

$$= \exp\left(i\frac{\pi}{2}\sigma_x^i\right)\cdot\exp(-i\alpha^{ij}\sigma_z^i\sigma_z^j t/\mathrm{h})\cdot\exp\left(-i\frac{\pi}{2}\sigma_x^i\right) \quad \text{Eq. (S.2-6b)}$$

$$= \exp\left(-i\frac{\pi}{2}\sigma_y^i\right)\cdot\exp(-i\alpha^{ij}\sigma_z^i\sigma_z^j t/\mathrm{h})\cdot\exp\left(i\frac{\pi}{2}\sigma_y^i\right) \quad \text{Eq. (S.2-6c)}$$

$$= \exp\left(i\frac{\pi}{2}\sigma_y^i\right)\cdot\exp(-i\alpha^{ij}\sigma_z^i\sigma_z^j t/\mathrm{h})\cdot\exp\left(-i\frac{\pi}{2}\sigma_y^i\right) \quad \text{Eq. (S.2-6d)}$$

Any decomposed operation sets can be chosen for the pulse sequence in Eqs. (S.2-6). If you do not care about the global phase, any pattern of $\pi$ pulses with the same direction is permitted as given by Eqs. (S.2-7).

$$-\exp(i\alpha^{ij}\sigma_z^i\sigma_z^j t/\mathrm{h}) = \exp\left(-i\frac{\pi}{2}\sigma_x^i\right)\cdot\exp(-i\alpha^{ij}\sigma_z^i\sigma_z^j t/\mathrm{h})\cdot\exp\left(-i\frac{\pi}{2}\sigma_x^i\right) \quad \text{Eq. (S.2-7a)}$$

$$= \exp\left(i\frac{\pi}{2}\sigma_x^i\right)\cdot\exp(-i\alpha^{ij}\sigma_z^i\sigma_z^j t/\mathrm{h})\cdot\exp\left(i\frac{\pi}{2}\sigma_x^i\right) \quad \text{Eq. (S.2-7b)}$$

$$= \exp\left(-i\frac{\pi}{2}\sigma_y^i\right)\cdot\exp(-i\alpha^{ij}\sigma_z^i\sigma_z^j t/\mathrm{h})\cdot\exp\left(-i\frac{\pi}{2}\sigma_y^i\right) \quad \text{Eq. (S.2-7c)}$$

$$= \exp\left(i\frac{\pi}{2}\sigma_y^i\right)\cdot\exp(-i\alpha^{ij}\sigma_z^i\sigma_z^j t/\mathrm{h})\cdot\exp\left(i\frac{\pi}{2}\sigma_y^i\right) \quad \text{Eq. (S.2-7d)}$$

An example of the pulse sequence is shown in Figure S4, being composed of Eqs. (S.2-3b), (S.2-4b) and (S.2-6c).

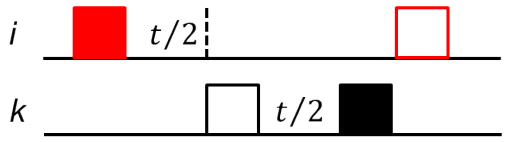


Figure S4. An example of the pulse sequence of a two spin interaction. The operation $\exp(i\alpha^{ij}\sigma_z^i\sigma_z^j t/\mathrm{h})$ ( $i\neq k, k\neq j, j\neq i$ ) is composed of Eqs. (S.2-3b), (S.2-4b) and (S.2-6c). The time is delimited by a dotted line.

**2.3.** A three spin interaction.

In general, *n* spin interactions can be simulated by two spin operations. Here, we show a 3 spin interaction case which can be expanded into the *n* spin interactions. At first, the three spin interaction is decomposed as given by Eqs. (S.2-8).

$$\exp(-i\alpha^{12}\sigma_z^1\sigma_z^2\sigma_z^3 t/\mathsf{h}) = \exp\left(-i\frac{\pi}{4}\sigma_x^1\right)\cdot\exp(-i\alpha^{12}\sigma_y^1\sigma_z^2\sigma_z^3 t/\mathsf{h})\cdot\exp\left(i\frac{\pi}{4}\sigma_x^1\right) \quad \text{Eq. (S.2-8a)}$$

$$= \exp\left(-i\frac{\pi}{4}\sigma_x^1\right)\cdot\exp\left(i\frac{\pi}{4}\sigma_x^1\sigma_z^3\right)\cdot\exp(-i\alpha^{12}\sigma_z^1\sigma_z^2 t/\mathsf{h})\cdot\exp\left(-i\frac{\pi}{4}\sigma_x^1\sigma_z^3\right)\cdot\exp\left(i\frac{\pi}{4}\sigma_x^1\right) \quad \text{Eq. (S.2-8b)}$$

$$= \exp\left(-i\frac{\pi}{4}\sigma_x^1\right)\cdot\exp\left(-i\frac{\pi}{4}\sigma_y^1\right)\cdot\exp\left(i\frac{\pi}{4}\sigma_z^1\sigma_z^3\right)\cdot\exp\left(i\frac{\pi}{4}\sigma_y^1\right)\cdot\exp(-i\alpha^{12}\sigma_z^1\sigma_z^2 t/\mathsf{h})$$

$$\cdot\exp\left(-i\frac{\pi}{4}\sigma_y^1\right)\cdot\exp\left(-i\frac{\pi}{4}\sigma_z^1\sigma_z^3\right)\cdot\exp\left(i\frac{\pi}{4}\sigma_y^1\right)\cdot\exp\left(i\frac{\pi}{4}\sigma_x^1\right) \quad \text{Eq. (S.2-8c)}$$

Obviously, there are other two expressions (Eqs. (S.2-9) to (S.2-12)) for Eq. (S.2-8c).

$$= \exp\left(-i\frac{\pi}{4}\sigma_x^2\right)\cdot\exp\left(-i\frac{\pi}{4}\sigma_y^2\right)\cdot\exp\left(i\frac{\pi}{4}\sigma_z^1\sigma_z^2\right)\cdot\exp\left(i\frac{\pi}{4}\sigma_y^2\right)\cdot\exp(-i\alpha^{12}\sigma_z^2\sigma_z^3 t/\mathsf{h})$$

$$\cdot\exp\left(-i\frac{\pi}{4}\sigma_y^2\right)\cdot\exp\left(-i\frac{\pi}{4}\sigma_z^1\sigma_z^2\right)\cdot\exp\left(i\frac{\pi}{4}\sigma_y^2\right)\cdot\exp\left(i\frac{\pi}{4}\sigma_x^2\right) \quad \text{Eq. (S.2-9)}$$

$$t = \alpha^{23}t'/\alpha^{12} \quad \text{Eq. (S.2-10)}$$

$$= \exp\left(-i\frac{\pi}{4}\sigma_x^3\right)\cdot\exp\left(-i\frac{\pi}{4}\sigma_y^3\right)\cdot\exp\left(i\frac{\pi}{4}\sigma_z^2\sigma_z^3\right)\cdot\exp\left(i\frac{\pi}{4}\sigma_y^3\right)\cdot\exp(-i\alpha^{12}\sigma_z^1\sigma_z^3 t/\mathsf{h})$$

$$\cdot\exp\left(-i\frac{\pi}{4}\sigma_y^3\right)\cdot\exp\left(-i\frac{\pi}{4}\sigma_z^2\sigma_z^3\right)\cdot\exp\left(i\frac{\pi}{4}\sigma_y^3\right)\cdot\exp\left(i\frac{\pi}{4}\sigma_x^3\right) \quad \text{Eq. (S.2-11)}$$

$$t = \alpha^{13}t'/\alpha^{12} \quad \text{Eq. (S.2-12)}$$

Note that *t'* and *t''* whose absolute value indicates the evolution time which can range to negative values. In this case, adopt Eqs. (S.2-6) in order to transform the positive time evolution. For the operation of $\exp(i\alpha^{12}\sigma_z^1\sigma_z^2\sigma_z^3 t/\mathsf{h})$, one can use the same procedure as given by Eqs. (S.2-6). The pulse sequence of Eq. (S.2-8c) with Eqs. (S.2-3b), (S.2-4b) and (S.2-6b) is shown in Figure S5. In this pulse sequence, the sign of $\alpha^{13}$ is assumed to be positive.

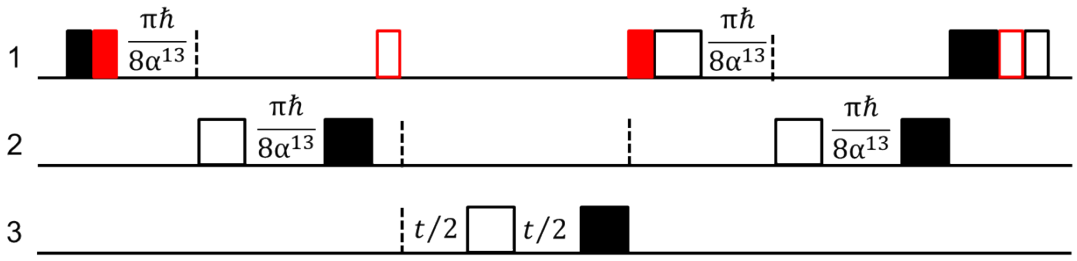


Figure S5. The pulse sequence of a three spin interaction. The operation $\exp(-i\alpha^{12}\sigma_z^1\sigma_z^2\sigma_z^3 t/\mathrm{h})$ is composed of Eqs. (S.2-3b), (S.2-4b), (S.2-6b) and (S.2-8c). $\alpha^{13}>0$ is assumed in this pulse sequence scheme. The time is delimited by a dotted line in 2 and 3.

**2.4.** The two spin interaction between the nuclei.

In one electron and two nuclear spin system, the spin interaction between the nuclei is too weak to perform the quantum gate operation. Therefore, this interaction (say $\sigma_z^2\sigma_z^3$ interaction) is replaced by other spin operations. Utilizing Eqs. (S.2-8c) and (S.2-10),

$$\begin{aligned}\exp(-i\alpha^{12}\sigma_z^2\sigma_z^3 t/\mathrm{h}) = {} & \exp\left(-i\frac{\pi}{4}\sigma_y^2\right)\cdot\exp\left(-i\frac{\pi}{4}\sigma_z^1\sigma_z^2\right)\cdot\exp\left(i\frac{\pi}{4}\sigma_y^2\right)\cdot\exp\left(i\frac{\pi}{4}\sigma_x^2\right)\cdot\exp\left(-i\frac{\pi}{4}\sigma_x^1\right)\\ & \cdot\exp\left(-i\frac{\pi}{4}\sigma_y^1\right)\cdot\exp\left(i\frac{\pi}{4}\sigma_z^1\sigma_z^3\right)\cdot\exp\left(-i\alpha^{12}\sigma_z^1\sigma_z^2 t/\mathrm{h}\right)\exp\left(-i\frac{\pi}{4}\sigma_y^1\right)\cdot\exp\left(-i\frac{\pi}{4}\sigma_z^1\sigma_z^3\right)\cdot\exp\left(i\frac{\pi}{4}\sigma_y^1\right)\\ & \cdot\exp\left(i\frac{\pi}{4}\sigma_x^1\right)\cdot\exp\left(-i\frac{\pi}{4}\sigma_x^2\right)\cdot\exp\left(-i\frac{\pi}{4}\sigma_y^2\right)\cdot\exp\left(i\frac{\pi}{4}\sigma_z^1\sigma_z^2\right)\cdot\exp\left(i\frac{\pi}{4}\sigma_y^2\right)\end{aligned} \qquad \text{Eq. (S.2-13)}$$

is obtained. The pulse sequence is shown in Figure S6 when the sign of $\alpha^{12}$ and $\alpha^{13}$ are positive and adopting Eqs. (S.2-3b), (S.2-4b) and (S.2-6b).

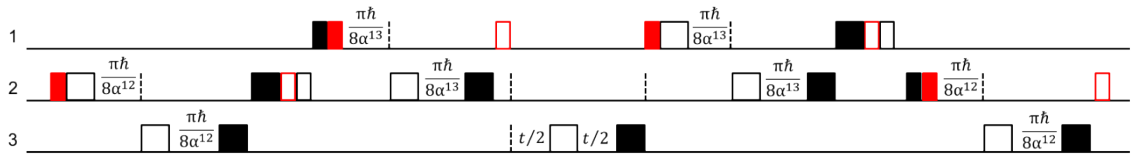


Figure S6. The pulse sequence of a three spin interaction. The operation $e^{-\alpha^{12}\sigma_z^2\sigma_z^3 t/\mathrm{h}}$ is composed of Eqs. (S.2-3b), (S.2-4b), (S.2-6b) and (S.2-13). $\alpha^{12},\alpha^{13}>0$ are assumed in this pulse sequence scheme. The time is delimited by a dotted line in 2 and 3.

**2.5.** The calculation method of the AQC pulse sequence.

The quantum path of the adiabatic factorization algorithm of 21 is defined by the time evolution of the initial Hamiltonian (Eq. (S.2-14)) and the final Hamiltonian (Eq. (S.2-15)).

$$H_{\mathrm{in}} / \mathsf{h} = a(\sigma_x^1 + \sigma_x^2 + \sigma_x^3)\ ,\ a = 30 \qquad \text{Eq. (S.2-14)}$$

$$H_{\mathrm{f}} / \mathsf{h} = (21 - xy)^2\ ,\ x = (I - \sigma_z^1) + I\ ,\ y = 2(I - \sigma_z^2) + (I - \sigma_z^3) + I \qquad \text{Eq. (S.2-15)}$$

Eq. (S.2-15) are expanded to the Eq. (S.2-16).

$$\begin{aligned} H_{\mathrm{f}} / \mathsf{h} &= 210I + 84\sigma_z^1 + 88\sigma_z^2 + 44\sigma_z^3 - 20\sigma_z^1\sigma_z^2 - 10\sigma_z^1\sigma_z^3 + 20\sigma_z^2\sigma_z^3 - 16\sigma_z^1\sigma_z^2\sigma_z^3 \\ &\sim 210I + 84\sigma_z^1 + 88\sigma_z^2 + 44\sigma_z^3 - 20\sigma_z^1\sigma_z^2 - 10\sigma_z^1\sigma_z^3 + 20\sigma_z^2\sigma_z^3 - 16\sigma_z^1\sigma_z^2\sigma_z^3 \end{aligned} \qquad \text{Eq. (S.2-16)}$$

The time evolution of this algorithm is defined by Eq. (S.2-17).

$$U = \prod_{m=1}^{5} \exp(-iH_m \Delta t / \mathsf{h})\ ,\ H_m = (m/5)^2 H_{\mathrm{f}} + \{1 - (m/5)^2 H_{\mathrm{i}}\ ,\ \Delta t = 0.028 \qquad \text{Eq. (S.2-17)}$$

In the pulse sequence scheme, we calculated the Trotter formula (Eq. (S2-18)) due to the non-commutativity of $H_{\mathrm{i}}$ (Eq. (S.2-14)) and $H_{\mathrm{f}}$ (Eq. (S.2-16)).

$$U = \prod_{m=1}^{5} \exp(-i\{1 - (m/5)^2\} H_{\mathrm{i}} \Delta t / 2\mathsf{h}) \cdot \exp(-i(m/5)^2 H_{\mathrm{f}} \Delta t / \mathsf{h}) \cdot \exp(-i\{1 - (m/5)^2\} H_{\mathrm{i}} \Delta t / 2\mathsf{h}) \qquad \text{Eq. (S.2-18)}$$

The pulse sequence was calculated by replacing each operator (single spin operation, two spin interaction and three spin interaction) for the AQC pulse sequence. The method for representing each operator is given in the section S2.1 to S2.4. In this calculation, the three spin interaction and the two spin interaction between nuclei are fixed for Eqs. (S.2-8c) and (S.2-13). In the time evolution of the spin system, we did not adopt Eq. (S.2-3a) but Eq. (S.2-3b). In order to make the pulse sequence simpler, some pulses are replaced by the other pulses. This simplification is performed when the two pulses for the same spin and the same direction can be combined to one pulse.

## 3. The interaction tensor of the phthalocyanine system.

The Mg-centered phthalocyanine system with three electron spin sites is adopted for a molecular spin QC on which AQC is performed. This molecule has one reduced spin site of -N–O–H and three N–O• radical sites, as illustrated in Figure S7. The geometry optimization was carried out at the UB3LYP/6-31G* level of theory using Gaussian 03 software [S1]. No imaginary vibrational frequency was obtained at the optimized geometry. The molecule belongs to a $C_s$ point group with a mirror plane parallel to the HON...Mg...NO• axis. The Cartesian coordinates of the optimized geometry are given in Table S1.

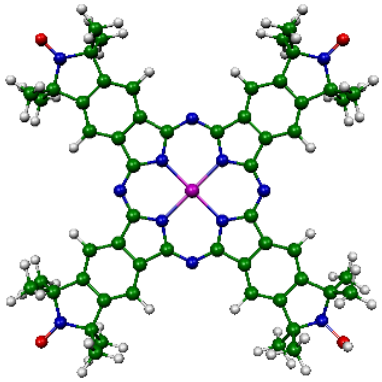

Figure S7. The optimized structure of the phthalocyanine triradical molecule.

Table S1. Cartesian coordinates of the phthalocyanine triradical molecule.

| Atom | X | Y | Z |
|---|---|---|---|
| Mg | 0.008958 | −0.019699 | 0.000000 |
| O | 0.003806 | −0.016478 | −10.050065 |
| O | −0.024926 | −10.070140 | 0.000000 |
| O | 0.003806 | −0.016478 | 10.050065 |
| O | 0.029874 | 10.076190 | 0.000000 |
| N | 0.014208 | 1.987889 | 0.000000 |
| N | 0.016697 | 2.376187 | −2.395392 |
| N | 0.008002 | −0.020026 | −2.007912 |
| N | −0.000666 | −2.415795 | −2.396166 |
| N | 0.016697 | 2.376187 | 2.395392 |
| N | 0.008002 | −0.020026 | 2.007912 |
| N | 0.000876 | −2.028049 | 0.000000 |
| N | −0.000666 | −2.415795 | 2.396166 |
| N | 0.004310 | −0.017128 | 8.776148 |
| N | −0.021558 | −8.796229 | 0.000000 |
| N | 0.004310 | −0.017128 | −8.776148 |

| | | | |
|---|---|---|---|
| N | 0.410563 | 8.716304 | 0.000000 |
| C | 0.025079 | 4.177831 | 0.707141 |
| C | 0.025079 | 4.177831 | −0.707141 |
| C | 0.018411 | 2.776434 | −1.123427 |
| C | 0.018411 | 2.776434 | 1.123427 |
| C | 0.012125 | 1.103664 | −2.795037 |
| C | 0.010553 | 0.687553 | −4.196346 |
| C | 0.004783 | −0.726813 | −4.196970 |
| C | 0.003644 | −1.143913 | −2.795962 |
| C | −0.001573 | −2.815765 | −1.123725 |
| C | 0.012125 | 1.103664 | 2.795037 |
| C | 0.003644 | −1.143913 | 2.795962 |
| C | 0.004783 | −0.726813 | 4.196970 |
| C | 0.010553 | 0.687553 | 4.196346 |
| C | −0.005671 | −4.216680 | −0.707246 |
| C | −0.005671 | −4.216680 | 0.707246 |
| C | −0.001573 | −2.815765 | 1.123725 |
| C | −0.008979 | −5.409322 | −1.432608 |
| C | −0.012314 | −6.596577 | −0.706449 |
| C | −0.012314 | −6.596577 | 0.706449 |
| C | −0.008979 | −5.409322 | 1.432608 |
| C | 0.013885 | 1.413652 | −5.388404 |
| C | 0.010698 | 0.688102 | −6.576132 |
| C | 0.004176 | −0.724686 | −6.576838 |
| C | 0.001404 | −1.451547 | −5.389878 |
| C | 0.035290 | 5.370102 | 1.433672 |
| C | 0.041783 | 6.555963 | 0.705444 |
| C | 0.041783 | 6.555963 | −0.705444 |
| C | 0.035290 | 5.370102 | −1.433672 |
| C | 0.001404 | −1.451547 | 5.389878 |
| C | 0.004176 | −0.724686 | 6.576838 |
| C | 0.010698 | 0.688102 | 6.576132 |
| C | 0.013885 | 1.413652 | 5.388404 |
| C | 0.000984 | −1.280022 | 7.985773 |
| C | 0.013614 | 1.244912 | 7.984474 |

| | | | |
|---|---|---|---|
| C | −0.016245 | −8.005233 | −1.262491 |
| C | −0.016245 | −8.005233 | 1.262491 |
| C | 0.013614 | 1.244912 | −7.984474 |
| C | 0.000984 | −1.280022 | −7.985773 |
| C | 0.033476 | 7.976423 | 1.239444 |
| C | 0.033476 | 7.976423 | −1.239444 |
| C | 1.263280 | −2.095012 | 8.322988 |
| C | −1.267335 | −2.086444 | 8.320689 |
| C | −1.246172 | 2.064709 | 8.319132 |
| C | 1.284390 | 2.047232 | 8.320213 |
| C | −1.281062 | −8.336642 | 2.075823 |
| C | 1.249537 | −8.345202 | 2.070915 |
| C | 1.249537 | −8.345202 | −2.070915 |
| C | −1.281062 | −8.336642 | −2.075823 |
| C | −1.267335 | −2.086444 | −8.320689 |
| C | 1.263280 | −2.095012 | −8.322988 |
| C | 1.284390 | 2.047232 | −8.320213 |
| C | −1.246172 | 2.064709 | −8.319132 |
| C | −1.356013 | 8.345171 | −1.812232 |
| C | 1.112394 | 8.239980 | −2.301680 |
| C | 1.112394 | 8.239980 | 2.301680 |
| C | −1.356013 | 8.345171 | 1.812232 |
| H | −0.008905 | −5.396162 | −2.518577 |
| H | −0.008905 | −5.396162 | 2.518577 |
| H | 0.019038 | 2.499595 | −5.374439 |
| H | −0.003207 | −2.537513 | −5.377330 |
| H | 0.041514 | 5.356349 | 2.519593 |
| H | 0.041514 | 5.356349 | −2.519593 |
| H | −0.003207 | −2.537513 | 5.377330 |
| H | 0.019038 | 2.499595 | 5.374439 |
| H | 1.283771 | −2.300902 | 9.397409 |
| H | 2.169721 | −1.543011 | 8.055578 |
| H | 1.263807 | −3.046222 | 7.779996 |
| H | −1.291021 | −2.292475 | 9.395015 |
| H | −1.273444 | −3.037486 | 7.777460 |

| | | | |
|---|---|---|---|
| H | −2.169471 | −1.528069 | 8.051939 |
| H | −1.267474 | 2.271546 | 9.393356 |
| H | −2.154194 | 1.515695 | 8.050882 |
| H | −1.242395 | 3.015499 | 7.775397 |
| H | 1.307196 | 2.254773 | 9.394273 |
| H | 1.294864 | 2.997365 | 7.775488 |
| H | 2.184912 | 1.485237 | 8.053660 |
| H | −1.306435 | −9.410864 | 2.282204 |
| H | −2.185520 | −8.065654 | 1.522312 |
| H | −1.280623 | −7.793230 | 3.026795 |
| H | 1.268312 | −9.419505 | 2.277586 |
| H | 1.256642 | −7.801408 | 3.021629 |
| H | 2.153663 | −8.080639 | 1.513765 |
| H | 1.268312 | −9.419505 | −2.277586 |
| H | 2.153663 | −8.080639 | −1.513765 |
| H | 1.256642 | −7.801408 | −3.021629 |
| H | −1.306435 | −9.410864 | −2.282204 |
| H | −1.280623 | −7.793230 | −3.026795 |
| H | −2.185520 | −8.065654 | −1.522312 |
| H | −1.291021 | −2.292475 | −9.395015 |
| H | −2.169471 | −1.528069 | −8.051939 |
| H | −1.273444 | −3.037486 | −7.777460 |
| H | 1.283771 | −2.300902 | −9.397409 |
| H | 1.263807 | −3.046222 | −7.779996 |
| H | 2.169721 | −1.543011 | −8.055578 |
| H | 1.307196 | 2.254773 | −9.394273 |
| H | 2.184912 | 1.485237 | −8.053660 |
| H | 1.294864 | 2.997365 | −7.775488 |
| H | −1.267474 | 2.271546 | −9.393356 |
| H | −1.242395 | 3.015499 | −7.775397 |
| H | −2.154194 | 1.515695 | −8.050882 |
| H | −1.382310 | 9.397057 | −2.117852 |
| H | −2.165010 | 8.161332 | −1.097663 |
| H | −1.563148 | 7.738761 | −2.699884 |
| H | 1.150056 | 9.310931 | −2.526766 |

| | | | |
|---|---|---|---|
| H | 0.899302 | 7.699647 | −3.231540 |
| H | 2.093331 | 7.932836 | −1.929445 |
| H | 1.150056 | 9.310931 | 2.526766 |
| H | 2.093331 | 7.932836 | 1.929445 |
| H | 0.899302 | 7.699647 | 3.231540 |
| H | −1.382310 | 9.397057 | 2.117852 |
| H | −1.563148 | 7.738761 | 2.699884 |
| H | −2.165010 | 8.161332 | 1.097663 |
| H | −0.949031 | 10.105495 | 0.000000 |

**3.1.** The zero field splitting tensor of the phthalocyanine system.

The zero field splitting (*D*-) tensor of the phthalocyanine system (Figure S8) was calculated in the point dipole approximation (Eq. (S.3-1)). Here, $\theta$ is an angle between the static magnetic field and the line connecting two radical sites. The spin distance was assumed for the mean distance between N-N and O-O in the nitroxide radical moieties. Table S2 shows the spin distance and *D* tensors between the spin sites.

$$D/h = -\frac{3}{2}\frac{\mu_0(g\beta)^2}{4\pi r^3 h}, \qquad D_{zz} = D(3\cos^2\theta - 1) \qquad \text{Eq (S.3-1)}$$

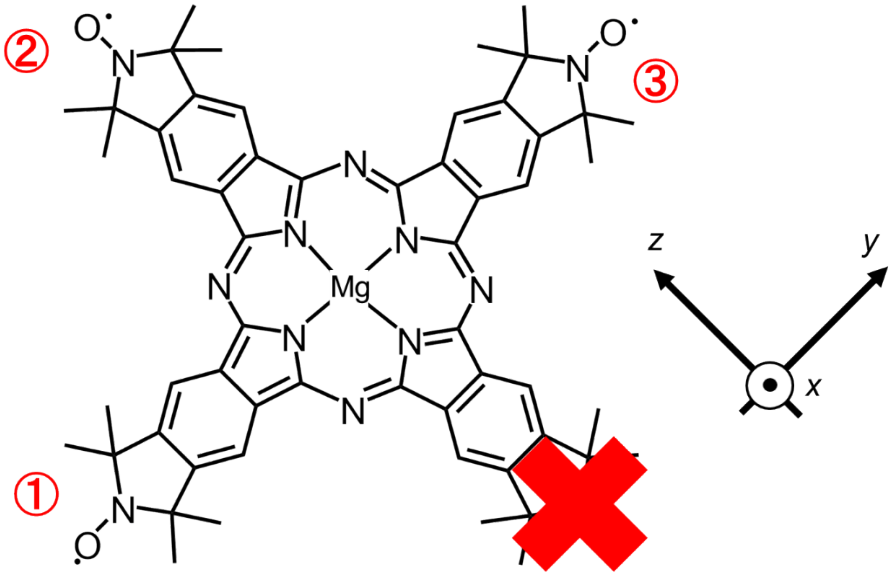


Figure S8. The molecular structure of the phthalocyanine system. The radical sites are designated by the red numbers.

Table S2. The spin distances and *D*-values of the zero field splitting tensor.

| | 1-2 | 2-3 | 3-1 |
|---|---|---|---|
| Distance /Å | 13.31 | 13.31 | 18.82 |
| $D/h$ /MHz | −33.11 | −33.11 | −11.71 |

**3.2.** The coupling constants of exchange interaction in the phthalocyanine system.

Exchange coupling constants $J$ in the phthalocyanine triradical system are calculated by means of the broken-symmetry DFT method [S2]. We emphasize that the originally proposed broken-symmetry scheme is limited to two-spin based singlet-triplet systems, and the extension of the broken-symmetry approach to three-spin triradical systems is not trivial [S3]. In this study, exchange coupling constants are derived by assuming a Heisenberg Hamiltonian acting on the unpaired electrons localized onto the NO sites, as follows:

$$H = -2J_{12}\mathbf{S}_1 \cdot \mathbf{S}_2 - 2J_{23}\mathbf{S}_2 \cdot \mathbf{S}_3 - 2J_{31}\mathbf{S}_3 \cdot \mathbf{S}_1 . \qquad \text{Eq. (S.3-2)}$$

The numbering of the spin site is given in Figure S8. The Heisenberg Hamiltonian matrix in the spin function (Slater determinant) basis ($|\alpha\alpha\beta\rangle$, $|\alpha\beta\alpha\rangle$, and $|\beta\alpha\alpha\rangle$) is written as follows:

$$H \rightarrow \begin{pmatrix} (-J_{12}+J_{23}+J_{31})/2 & -J_{23} & -J_{31} \\ -J_{23} & (J_{12}+J_{23}-J_{31})/2 & -J_{12} \\ -J_{31} & -J_{12} & (J_{12}-J_{23}+J_{31})/2 \end{pmatrix} \qquad \text{Eq. (S.3-3)}$$

According to the $C_s$ symmetry of the phthalocyanine molecule, we can safely assume as $J_{12} = J_{23}$. In this case the secular equation can be solved analytically, and the following eigenfunctions and eigenvalues of one spin-quartet and two spin-doublet states are obtained.

$$\Psi\left(S=\frac{3}{2}, M_S=\frac{1}{2}\right) = \frac{1}{\sqrt{3}}\left(|\alpha\alpha\beta\rangle + |\alpha\beta\alpha\rangle + |\beta\alpha\alpha\rangle\right),$$

$$E\left(S=\frac{3}{2}, M_S=\frac{1}{2}\right) = -(J_{12}+J_{23}+J_{31})/2 \qquad \text{Eq. (S.3-4)}$$

$$\Psi\left(S=\frac{1}{2}, M_S=\frac{1}{2};1\right) = \frac{1}{\sqrt{6}}\left(2|\alpha\beta\alpha\rangle - |\alpha\alpha\beta\rangle - |\beta\alpha\alpha\rangle\right),$$

$$E\left(S=\frac{1}{2}, M_S=\frac{1}{2};1\right) = J_{12}+J_{23}-J_{31}/2 \qquad \text{Eq. (S.3-5)}$$

$$\Psi\left(S=\frac{1}{2}, M_S=\frac{1}{2};2\right) = \frac{1}{\sqrt{2}}\left(|\alpha\alpha\beta\rangle - |\beta\alpha\alpha\rangle\right)$$

$$E\left(S=\frac{3}{2}, M_S=\frac{1}{2};2\right) = 3J_{31}/2 \qquad \text{Eq. (S.3-6)}$$

Here, $\Psi(S, M_S; X)$ represents an eigenfunction of the Heisenberg Hamiltonian of the spin quantum number $S$ and magnetic quantum number $M_S$. $X$ is introduced to differentiate between the two spin-doublet wavefunctions. Eqs. (S.3-4) to (S3-6) hold regardless of the absolute signs and magnitudes (ratios) of the $J$ values. (The off-diagonal term of the Heisenberg Hamiltonian between the two spin-

doublet eigenfunctions is calculated to be $\sqrt{3}(J_{12} - J_{23})/2$, which vanishes for $J_{12} = J_{23}$). The spin-doublet eigenfunctions in Eqs. (S.3-5) and (S.3-6) have multideterminantal characters and cannot be represented in terms of DFT directly. However, since the structure of the spin eigenfunctions is well defined in our case, we can derive energy differences between the spin states as well as the exchange coupling constants $J$ from the diagonal terms of the Heisenberg Hamiltonian Eq. (S.3-3). It should be emphasised that the calculations of the off-diagonal terms in the Heisenberg Hamiltonian is not straightforward in DFT, because Kohn–Sham orbitals are not identical between two determinants such as $|\alpha\alpha\beta\rangle$ and $|\alpha\beta\alpha\rangle$.

In this study, we have calculated one spin-quartet (**HS**, $M_S = 3/2$) and two broken-symmetry (**BS1** and **BS2**) states with $M_S = 1/2$ as illustrated in Figure S9. It should be noted that the reliable calculation of exchange coupling constants $J$ in terms of BS-DFT is very difficult because the level of accuracy strongly depends on the nature of the species under study, exchange–correlation functionals, and basis sets. In the present study we used the UB3LYP/6-31G* level of theory for the calculations because qualitative $J$ values can usually be obtained at this level. We checked exchange–correlation functional dependences of the $J$ values by using O3LYP, B3PW91, and BMK functionals, revealing that no significant differences in the trend of $J$ values are obtained (See Table S4). Change of the basis set from 6-31G* to 6-311G* causes no significant changes in the $J$ values as well. We also examined the validity of the present computations for weakly exchange-coupled systems using known TEMPO (2,2,6,6-tetramethylpiperidine 1-oxyl) biradicals **BIR-1** and **BIR-2** as illustrated in Figure S10 [S4,S5]. Note that the experiments were carried out using isotope-labelled samples for **BIR-1** and **BIR-2**, aiming to make ESR lines narrower and to make two TEMPO radicals distinguishable. Experimentally determined exchange coupling constants $J$ in the TEMPO biradicals are +0.07 MHz and less than 0.5 MHz (in absolute value) for **BIR-1** and **BIR-2**, respectively. Note that the Heisenberg exchange coupling Hamiltonian is defined as $H = J_{12}\mathbf{S}_1 \cdot \mathbf{S}_2$ in Refs. S4 and S5, not as $H = -2J_{12}\mathbf{S}_1 \cdot \mathbf{S}_2$. Therefore, we divided the $J$ value given in Refs. S4 and S5 by a factor of −2 for the purpose of direct comparison. At the UB3LYP/6-31G* level the $J$ value is calculated to be less than 0.07 MHz for **BIR-1**, and +2.50 MHz for **BIR-2**.

In the phthalocyanine-based triradical, energy separations among three (**HS**, **BS1**, and **BS2**) states are quite small (< $10^{-7}$ Hartree), we have adopted an ultrafine grid for the computations of two-electron integrals, and very tight SCF convergence criteria (requested convergence on RMS density matrix is $1.0 \times 10^{-12}$, max density matrix is $1.0 \times 10^{-10}$, energy is $1.0 \times 10^{-10}$ Hartree). The calculated DFT energies and $\langle S^2 \rangle$ values, and expected value of the Heisenberg Hamiltonian are summarised in Table S3. The exchange coupling constants $J$ were calculated by utilizing the following equations.

$$J_{12} = J_{23} = \{E(\mathbf{BS1}) - E(\mathbf{HS})\}/2 \qquad \text{Eq. (S.3-7)}$$

$$J_{31} = E(\mathbf{BS2}) - E(\mathbf{HS}) - J_{12} \qquad \text{Eq. (S.3-8)}$$

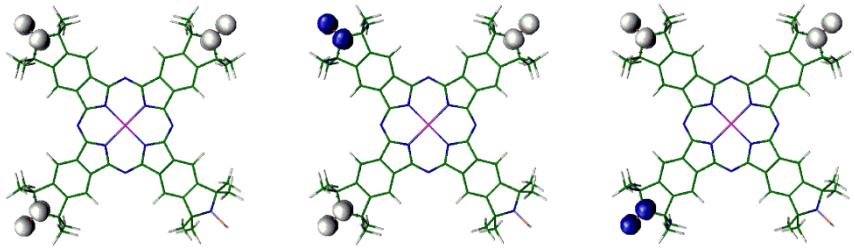


Figure S9. Contour plot of the spin density of a spin-quartet (**HS**) and two broken-symmetry (**BS1** and **BS2**) states. The isosurface value of the contour plot is set to 0.005.

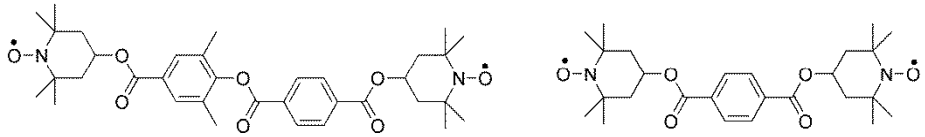

Figure S10. Weakly exchange-coupled TEMPO biradicals **BIR-1** (left) and **BIR-2** (right).

Table S3. The UB3LYP single point energies and $<S^2>$ values, and expectation value of the Heisenberg Hamiltonian.

| State | E(UB3LYP/6-31G*)/Hartree | $<S^2>$ | $<H$(Heisenberg)$>$ |
|---|---|---|---|
| **HS** | −3326.33031852657 | 3.7614 | $(-J_{12}-J_{23}-J_{31})/2$ |
| **BS1** | −3326.33031853021 | 1.7614 | $(J_{12}+J_{23}-J_{31})/2$ |
| **BS2** | −3326.33031853843 | 1.7614 | $(J_{12}-J_{23}+J_{31})/2$ |

Table S4. The exchange–correlation functional and basis set dependences of the exchange coupling constants *J*.

| Functional | Basis set | $J_{12}$/MHz | $J_{23}$/MHz | $J_{31}$/MHz |
|---|---|---|---|---|
| B3LYP | 6-31G* | −12.01 | −12.01 | −66.03 |
| O3LYP | 6-31G* | −8.03 | −8.03 | −54.02 |
| B3PW91 | 6-31G* | −14.21 | −14.21 | −47.83 |
| BMK | 6-31G* | −24.18 | −24.18 | −59.98 |
| B3LYP | 6-311G* | −17.30 | −17.30 | −51.65 |

**3.3.** The experimental axis of the static magnetic field in three electron system.

A static magnetic field direction is selected for the pulse sequence analysis. In order to have strong interactions between the spin sites, the static magnetic field is assumed to be along the z-direction as given in Figure S8. Table S5 shows the $D_{zz}$-values and the total coupling values $(D_{zz}+J)$ with Table S2 and S4.

Table S5. The interaction strength between the spin sites by theoretical calculation.

| | 1-2 | 2-3 | 3-1 |
|---|---|---|---|
| $\theta$ | $5\pi/4$ | $-5\pi/4$ | $\pi/2$ |
| $D_{zz}/h$ /MHz | −16.55 | −16.55 | 11.71 |
| $(D_{zz}+J)/h$ /MHz | −28.56 | −28.56 | −54.32 |

## 4. The interaction tensor of the glutaconic acid system.

Glutaconic acid has three nuclear spins and its radical produced by X-ray irradiation in the single crystal is known approximately to have collinear hyperfine tensors (Figure S11) [S6, S7]. In this study, we adopted the deuterated glutaconic acid (1st hydrogen atom is deuterated in Figure S11) for a molecular spin QC. In this system the direction of the static magnetic field is chosen to make the off-diagonal part of the hyperfine tensor small and the experimental values in the non-deuterated glutaconic acid is also given in the caption of Figure S11.

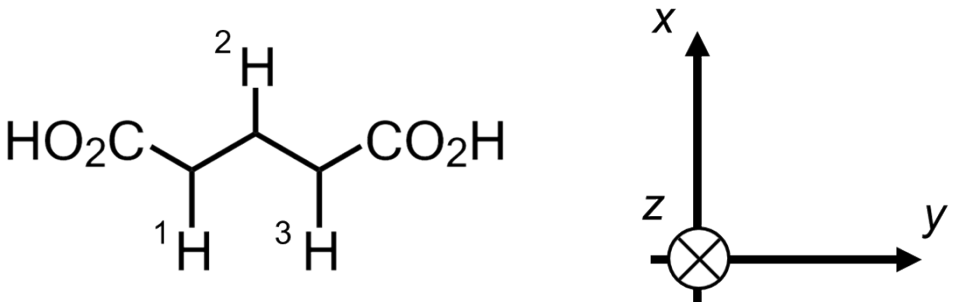


Figure S11. The molecular structure of the glutaconic acid radical. Deuterated The hydrogen 1 is deuterated and the direction of the static magnetic field is along the *z*-direction. The experimental principal values in *z*,*z*-direction of hyperfine tensors between the electron and 2nd and 3rd hydrogen nuclei are +7.0 MHz and −36.0 MHz, respectively.

## 5. The calculated pulse sequence in the single crystal ESR.

The pulse sequences for the phthalocyanine and glutaconic acid system are calculated by the method shown in section S2 taking into account of the global phase. The parameter of spin Hamiltonian in the phthalocyanine and glutaconic acid system is shown in section S3 and S4, respectively.

**5.1.** The 21 factorization pulse sequence for the phthalocyanine molecules.

The conquered pulse sequence for the factorization problem of 21 on the phthalocyanine molecule is given in Figure S12 and the calculation process of the sequence is shown in Figure S13. The detail of the blue pulse operation is given in Table S6 and S7. The required time was 0.1761 μs.

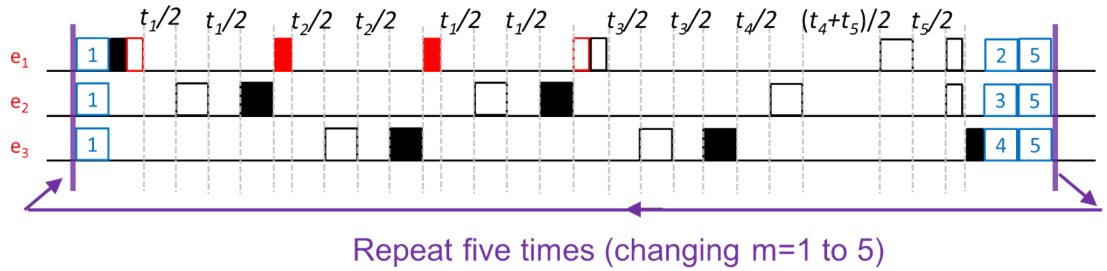


Figure S12. The pulse sequence for the phthalocyanine system. This sequence needs to repeat five times with changing the value of m=1 to 5 (see the section S2.5). The $e_1$, $e_2$ and $e_3$ correspond to the spin numbers of Figure S8. The notation of the black and red pulse blocks is shown in the section S2. The detail information on the pulse interval ( $t_1$ to $t_5$ ) and the blue blocks are shown in Table S6 and S7.

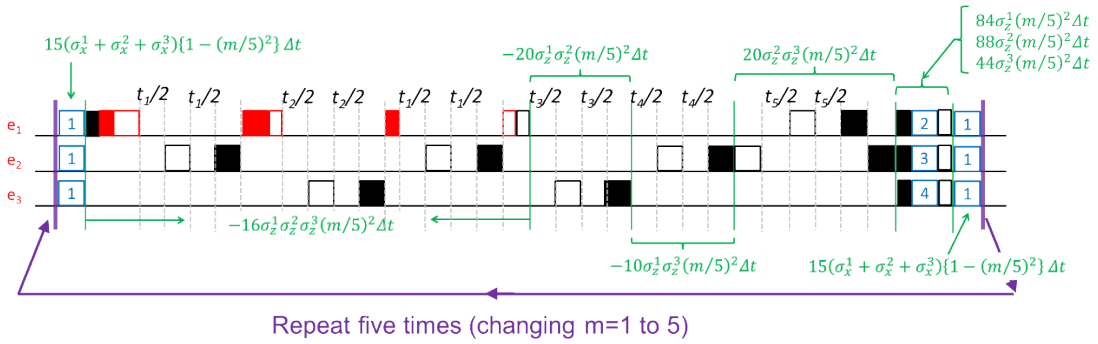


Figure S13. The calculation process of the pulse sequence in the phthalocyanine system. Relevant to the pulse operations of this Figure, the simplified pulse sequence (=Figure S12) is obtained. The notation is the same as in Figure S12, and the green letters indicate the AQC operations.

Table S6. The pulse interval of the phthalocyanine system. A) The analytical pulse interval ($t_1$ to $t_5$) in the phthalocyanine system. Here, $a_{\mathrm{m}} = 0.028\mathrm{h}(m/5)^2$. B) The obtained value of the pulse interval ($t_1$ to $t_5$) in the phthalocyanine system.

A)

| $t_1$ /s | $t_2$ /s | $t_3$ /s | $t_4$ /s | $t_5$ /s |
|---|---|---|---|---|
| $-\pi\mathrm{h}/(D_{zz}+J)^{13}$ | $-64a_m/(D_{zz}+J)^{12}$ | $-80a_m/(D_{zz}+J)^{12}$ | $-40a_m/(D_{zz}+J)^{13}$ | $-80a_m/(D_{zz}+J)^{23}$ |

B)

| | $t_1$ /ns | $t_2$ /ns | $t_3$ /ns | $t_4$ /ns | $t_5$ /ns |
|---|---|---|---|---|---|
| $m=1$ | 9.158 | 0.4017 | 0.5021 | 0.1306 | 0.5021 |
| $m=2$ | 9.158 | 1.607 | 2.008 | 0.5224 | 2.008 |
| $m=3$ | 9.158 | 3.615 | 4.519 | 1.175 | 4.519 |
| $m=4$ | 9.158 | 6.427 | 8.034 | 2.089 | 8.034 |
| $m=5$ | 9.158 | 10.04 | 12.55 | 3.265 | 12.55 |

Table S7. The rotational angles of the pulse operations. A) The analytical operation angles and the directions (Block 1 to 5) in the phthalocyanine system. Here, $b_{\mathrm{m}} = 0.028\{1-(m/5)^2\}$ and $c_{\mathrm{m}} = 0.028(m/5)^2$. B) The obtained value for the pulse operation angles (Block 1 to 5) in the phthalocyanine system. C) The total rotational angle for each spin in the phthalocyanine system.

A)

| 1 | 2 | 3 | 4 | 5 |
|---|---|---|---|---|
| $30b_{\mathrm{m}}$ | $168c_{\mathrm{m}}$ | $176c_{\mathrm{m}}$ | $88c_{\mathrm{m}}$ | $30b_{\mathrm{m}}+\pi/2$ |
| $x$ | $y$ | $y$ | $y$ | $x$ |

B)

| | 1 | 2 | 3 | 4 | 5 |
|---|---|---|---|---|---|
| $m=1$ | 0.8064 | 0.1882 | 0.1971 | 0.09856 | 2.377 |
| $m=2$ | 0.7056 | 0.7526 | 0.7885 | 0.3942 | 2.276 |
| $m=3$ | 0.5376 | 1.693 | 1.774 | 0.8870 | 2.108 |
| $m=4$ | 0.3024 | 3.011 | 3.154 | 1.577 | 1.873 |
| $m=5$ | 0 | 4.704 | 4.928 | 2.464 | 1.571 |

C)

| $\mathrm{e}_1$ | $\mathrm{e}_2$ | $\mathrm{e}_3$ |
|---|---|---|
| $29.79\pi$ | $34.95\pi$ | $28.22\pi$ |

**5.2.** The 21 factorization pulse sequence for the glutaconic acid molecules.

The conquered pulse sequence for the factorization problem of 21 by the glutaconic acid radical is shown in Figure S14, and the calculation process of the sequence is shown in Figure S15. The detail of the pulse operations for the glutaconic acid system is shown in Tables S8 and S9. The required time was 1.317 μs.

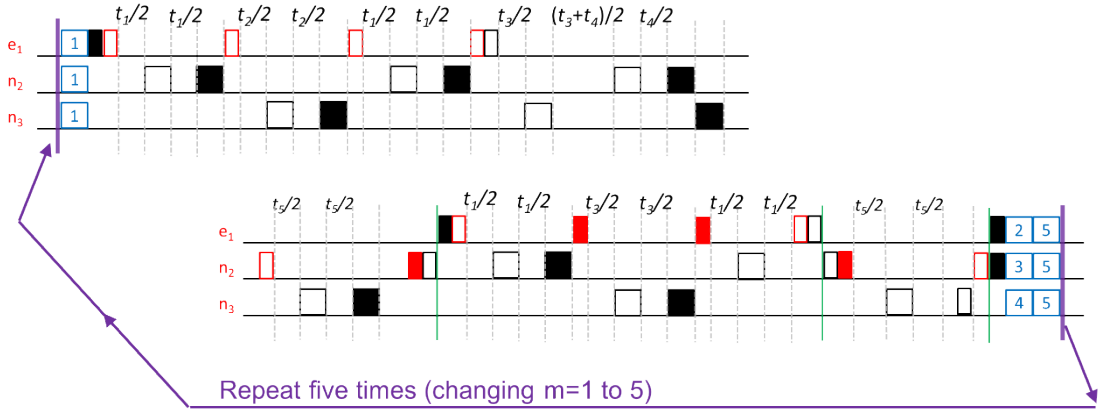


Figure S14. The pulse sequence for the glutaconic acid system. This sequence needs to repeat five times with changing the value of m=1 to 5 (see section S2.5). The $e_1$, $n_2$ and $n_3$ correspond to the spin numbers of Figure S11. The notation of the black and red pulse blocks is shown in section S2. The detail information about the pulse interval ($t_1$ to $t_5$) and the blue blocks are shown in Tables S8 and S9, respectively.

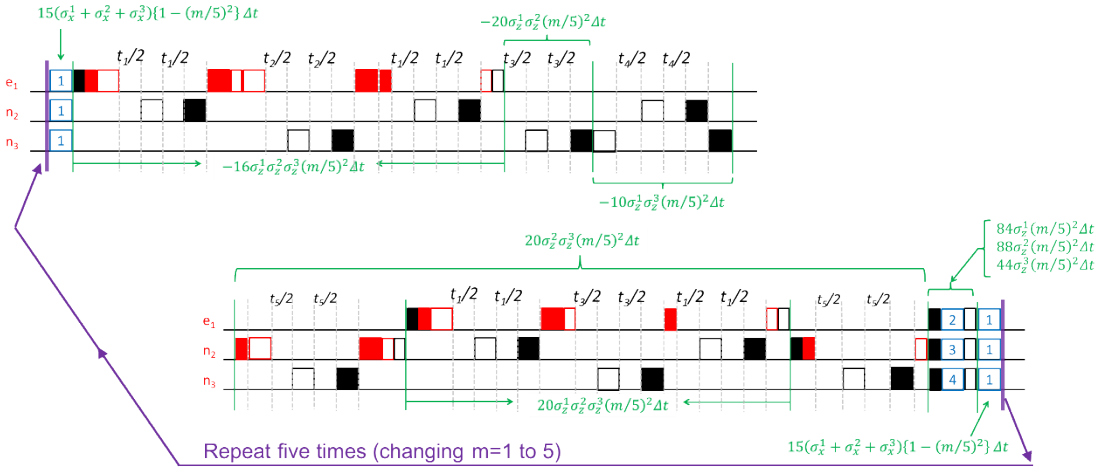


Figure S15. The calculation process of the pulse sequence in the glutaconic acid system. Relevant to the pulse operations of this Figure, the simplified pulse sequence (=Figure S14) is obtained. The notation is the same as in Figure S13, and the green letters indicate the AQC operations.

Table S8. The pulse interval of the glutaconic acid system. A) The analytical pulse interval ( $t_1$ to $t_5$ ) in the glutaconic acid system. Here, $a_{\mathrm{m}} = 0.028\mathrm{h}(m/5)^2$ . B) The obtained value of the pulse interval ( $t_1$ to $t_5$ ) in the glutaconic acid system.

A)

| $t_1$ /s | $t_2$ /s | $t_3$ /s | $t_4$ /s | $t_5$ /s |
|---|---|---|---|---|
| $-\pi\mathrm{h}/A_{zz}^{13}$ | $64a_m/A_{zz}^{12}$ | $80a_m/A_{zz}^{12}$ | $-40a_m/A_{zz}^{13}$ | $\pi\mathrm{h}/A_{zz}^{12}$ |

B)

| | $t_1$ /ns | $t_2$ /ns | $t_3$ /ns | $t_4$ /ns | $t_5$ /ns |
|---|---|---|---|---|---|
| $m=1$ | 13.89 | 1.630 | 2.037 | 0.1981 | 71.43 |
| $m=2$ | 13.89 | 6.519 | 8.149 | 0.7922 | 71.43 |
| $m=3$ | 13.89 | 14.67 | 18.33 | 1.783 | 71.43 |
| $m=4$ | 13.89 | 26.08 | 32.59 | 3.169 | 71.43 |
| $m=5$ | 13.89 | 40.74 | 50.93 | 4.951 | 71.43 |

Table S9. The rotational angles of the pulse operations. A) The analytical operation angles and the directions (Block 1 to 5) in the glutaconic acid system. Here, $b_{\mathrm{m}} = 0.028\{1-(m/5)^2\}$ and $c_{\mathrm{m}} = 0.028(m/5)^2$ . B) The obtained value of the pulse operation angles (Block 1 to 5) in the glutaconic acid system. C) The total rotational angle for each spin in the glutaconic acid system.

A)

| 1 | 2 | 3 | 4 | 5 |
|---|---|---|---|---|
| $30b_{\mathrm{m}}$ | $168c_{\mathrm{m}}$ | $176c_{\mathrm{m}}$ | $88c_{\mathrm{m}}$ | $30b_{\mathrm{m}}+\pi/2$ |
| $x$ | $y$ | $y$ | $y$ | $x$ |

B)

| | 1 | 2 | 3 | 4 | 5 |
|---|---|---|---|---|---|
| $m=1$ | 0.8064 | 0.1882 | 0.1971 | 0.09856 | 2.377 |
| $m=2$ | 0.7056 | 0.7526 | 0.7885 | 0.3942 | 2.276 |
| $m=3$ | 0.5376 | 1.693 | 1.774 | 0.8870 | 2.108 |
| $m=4$ | 0.3024 | 3.011 | 3.154 | 1.577 | 1.873 |
| $m=5$ | 0 | 4.704 | 4.928 | 2.464 | 1.571 |

C)

| $\mathrm{e}_1$ | $\mathrm{n}_2$ | $\mathrm{n}_3$ |
|---|---|---|
| $39.79\pi$ | $69.95\pi$ | $53.22\pi$ |

## 6. References.

[S1] M. J. Frisch, G. W. Trucks, H. B. Schlegel, G. E. Scuseria, M. A. Robb, J. R. Cheeseman, G. Scalmani, V. Barone, B. Mennucci, G. A. Petersson, H. Nakatsuji, M. Caricato, X. Li, H. P. Hratchian, A. F. Izmaylov, J. Bloino, G. Zheng, J. L. Sonnenberg, M. Hada, M. Ehara, K. Toyota, R. Fukuda, J. Hasegawa, M. Ishida, T. Nakajima, Y. Honda, O. Kitao, H. Nakai, T. Vreven, J. A. Montgomery Jr., J. E. Peralta, F. Ogliaro, M. Bearpark, J. J. Heyd, E. Brothers, K. N. Kudin, V. N. Staroverov, R. Kobayashi, J. Normand, K. Raghavachari, A. Rendell, J. C. Burant, S. S. Iyengar, J. Tomasi, M. Cossi, N. Rega, J. M. Millam, M. Klene, J. E. Knox, J. B. Cross, V. Bakken, C. Adamo, J. Jaramillo, R. Gomperts, R. E. Stratmann, O. Yazyev, A. J. Austin, R. Cammi, C. Pomelli, J. W. Ochterski, R. L. Martin, K. Morokuma, V. G. Zakrzewski, G. A. Voth, P. Salvador, J. J. Dannenberg, S. Dapprich, A. D. Daniels, O. Farkas, J. B. Foresman, J. V. Ortiz, J. Cioslowski and D. J. Fox, *GAUSSIAN 03 (Revision D.01)*, Gaussian Inc., Wallingford CT, 2004.

[S2] K. Yamaguchi, *Chem. Phys. Lett.,* 1975, **33**, 330–335.

[S3] M. Shoji, K. Koizumi, T. Hamamoto, T. Taniguchi, R. Takeda, Y. Kitagawa, T. Kawakami, M. Okumura, S. Yamanaka and K. Yamaguchi, *Polyhedron,* 2005, **24**, 2708–2715.

[S4] S. Nakazawa, S. Nishida, T. Ise, T. Yoshino, N. Mori, R. D. Rahimi, K. Sato, Y. Morita, K. Toyota, D. Shiomi, M. Kitagawa, H. Hara, P. Carl, P. Höfer and T. Takui, *Angew. Chem. Int. Ed.,* 2012, **124**, 9998–10002.

[S5] K. Ayabe, K. Sato, S. Nishida, T. Ise, S. Nakazawa, K. Sugisaki, Y. Morita, K. Toyota, D. Shiomi, M. Kitagawa and T. Takui, *Phys. Chem. Chem. Phys.,* 2012, **14**, 9137–9148.

[S6] C. Heller and T. Cole, *J. Chem. Phys*., 1962, **37**, 243–250.

[S7] H. R. Falle' and D. M. A. Whitehea, *Can. J. Chem*., 1972, **50**, 139–151.